Energetics of segregation and embrittling potency for non-transition elements in the Ni Σ5 (012) symmetrical tilt grain boundary: a first-principles study

2004 J. Phys.: Condens. Matter 16 3933

(http://iopscience.iop.org/0953-8984/16/23/013)

INSTITUTE OF PHYSICS PUBLISHING JOURNAL OF PHYSICS: CONDENSED MATTER

J. Phys.: Condens. Matter **16** (2004) 3933–3956 PII: S0953-8984(04)78845-1

Energetics of segregation and embrittling potency for non-transition elements in the Ni Σ5 (012) symmetrical tilt grain boundary: a first-principles study

Masatake Yamaguchi, Motoyuki Shiga and Hideo Kaburaki

Centre for Promotion of Computational Science and Engineering, Japan Atomic Energy Research Institute, Tokai-mura, Naka-gun, Ibaraki 319-1195, Japan

E-mail: yamagu@popsvr.tokai.jaeri.go.jp

Received 2 April 2004
Published 28 May 2004
Online at stacks.iop.org/JPhysCM/16/3933
DOI: 10.1088/0953-8984/16/23/013

Abstract

A series of non-transition elements bound to the Ni Σ5 (012) symmetrical tilt grain boundary (GB) and the (012) free surface (FS) systems has been studied by first-principles calculation using WIEN2k code, which is based on the full-potential linearized augmented plane wave method with the generalized gradient approximation. The multilayer relaxations in the presence and absence of solutes are determined by the force minimization procedure. The binding energies at some GB/FS/bulk sites including both interstitial and substitutional sites are calculated for all the non-transition elements between H and Rn (from the first-row to the sixth-row elements). The GB/FS segregation energy is obtained by calculating the binding energy difference between the GB/FS site and the inner bulk site. The embrittling potency energy is obtained by calculating the difference between the GB and FS segregation energies on the basis of the Rice–Wang model. The calculated results show that most of the non-transition elements have negative GB/FS segregation energies. In our definition, this means that there exists a segregation site in the GB/FS that is more stable for the solute atom than in the bulk. The embrittling potency energies are positive for most of the solutes. However, some exceptions such as Be, B, C, and Si having negative and large embrittling potency can enhance the GB cohesion. The calculated results are found to be consistent with the various experimental findings within the discussion based on the simple site competition model neglecting the interactions between different solutes.

1. Introduction

It is well known that a small amount of boron and carbon increases ductility while phosphorus and sulfur cause embrittlement in iron. Hydrogen also brings about embrittlement in transition

metals. In this way, solute or impurity atoms can make drastic changes in the mechanical strength of metallic materials. It is believed that one of the important factors in this phenomenon is the change in the cohesive energy of the grain boundary (GB) assisted by the segregation of the solute at the GB. However, the microscopic origin of the interaction between the GBs and solute atoms has not been clarified due to the limitations in experimental techniques.

As an alternative approach for resolving this problem, computer simulation is useful. In particular, recent progress in first-principles calculation has made it possible to simulate the electronic structure (bonding character) and the geometry (lattice distortion and binding sites) when the solute atom is present at the GB. In a pioneering work, Wu *et al* [1] evaluated the embrittling and strengthening effect of B, C, and P atoms in body-centred-cubic (bcc) Fe using a first-principles calculation based on the full-potential linearized augmented plane wave method (FLAPW) [2] within the local spin-density approximation. In this calculation, they defined the embrittling potency energy as the difference between the solute binding energy at the GB and that at the free surface (FS). The theoretical background in this work is based on the Rice–Wang model, in which the binding energy difference is considered to dominate embrittling/strengthening behaviour of the solute atom at the GB [3]. Originally, the Rice–Wang model describes the competition between the brittle boundary separation and the plastic crack blunting processes in the presence of solute atom segregation at the GB. For the former process, the resistance to brittle fracture is characterized by the thermodynamic work corresponding to the energy difference between the GB and FS. This means that if a solute atom prefers energetically being at the GB to being at the FS, the segregation of the solute atom may lower the energy necessary to cause intergranular fracture. The results calculated by Wu *et al* imply that B and C atoms have a strengthening effect on the GB while P has an embrittling effect. These findings are consistent with the experimental observations. Using a similar method, Freeman and co-workers have calculated the embrittling potency energies of the other types of systems, such as H atoms in the Fe $\Sigma 3$ (111) GB and H, B, P, Li, He, and Ca atoms in the Ni $\Sigma 5$ (012) GB [4–10].

Geng *et al* [9] showed that the embrittling potency of H in the Ni $\Sigma 5$ (012) GB was about 0.3 eV/H atom when H was placed at a grain boundary vacancy site (GB0 site). Using a first-principles calculation similar to that used by them, we studied the same system in more detail [11]. The slight difference in the calculation method is that we use WIEN2k code which adopts three-dimensional periodic boundary conditions, whereas they use the *film*-FLAPW code in which only two-dimensional boundary conditions are required. The merit of their *film* method is that it avoids the unrealistic interaction among interfaces in the GB or FS. However, if the unit cell size is taken to be sufficiently large, the interaction between the interfaces would be negligible even with three-dimensional periodic boundary conditions. Careful treatment of the geometry optimization procedure revealed that the most stable geometry of the H atom in the GB plane was different from the GB0 site. However, our redetermined embrittling potency energy was also about 0.3 eV/H atom, which is very close to the result of Geng *et al*. In addition, we estimated the GB/FS segregation energy given by the difference between the binding energy of the solute atom at the GB/FS site and that at the inner bulk site. The calculated GB and FS segregation energies have been evaluated to be -0.3 and -0.6 eV/H atom, respectively. (Here, the negative values imply that the H atom prefers the GB and FS sites to the inner bulk site in our definition.) Furthermore, we calculated the quantum mechanical zero-point energy of the H atom at the GB, FS, and inner bulk sites. The zero-point energy results were within the range of 0.12–0.16 eV/H atom at all sites, indicating that the zero-point correction has some influence on binding energies on each site. However, on the whole, it does not have a significant effect on the GB/FS segregation energy and embrittling potency energy. On the other hand, we calculated the binding energy and embrittling potency energy of H atoms

in many symmetrical tilt GBs (Σ5, Σ7, Σ9, Σ11, ...) of Ni using the embedded atom method (EAM), which is a semiempirical calculation rather than a first-principles one [12]. For all the types of GBs studied, it was found that H atom had a positive embrittling potency energy about 0.3 eV/H atom. From our first-principles and EAM calculations, we concluded that hydrogen had an effect of segregating and embrittling the symmetrical tilt GBs of Ni according to the Rice–Wang model.

Geng *et al* [13] employed a phenomenological method for rough estimations of the embrittling potency energies of various solute elements in the Fe Σ3 and Ni Σ5 GBs. In their parametrization, they took three quantities, atomic size, bonding character, and heat of formation for solid solutions, which were taken from either the classical theory or their own first-principles calculations. Their results showed that some transition elements had negative values of embrittling potency energies, which means that they have strengthening character as regards the GB.

Recently, several more investigations on grain boundary systems including solute atoms or impurities have been reported [14–19]. For example, Wang and Wang [14] investigated the bonding characters of boron (B) and sulfur (S) in Ni clusters. They showed that B formed strong covalent bondings with Ni while S did not. For another example, Janisch and Elsässer calculated the electronic structures of the bcc Nb and Mo Σ5 (310) symmetrical tilt GB including some light elements (B, C, N, and O) by a mixed-basis pseudopotential approach [19]. They showed that B and C formed angle-dependent covalent-like bonds across the interface and favoured a mirror-symmetric configuration, while N and O as well as H formed isotropic polar-like bonds and broke the mirror symmetry leading to interfacial embrittlement. They insisted that, on the basis of the energetical trends concerning cohesion of boundaries and embrittlement by segregation in bcc transition metals, their results supported the qualitative validity of empirical models suggested by Cottrel [20] and Rice and Wang [3].

In this paper, we report first-principles calculations using WIEN2k code for the symmetrical tilt Ni Σ5 (012) GB and Ni (012) FS with various kinds of impurity atoms. To our knowledge, this is the first work that has studied the GB/FS segregation energies for the series of all non-transition elements by means of systematic first-principles calculations along with comparison with experimental data. The embrittling potency energy, which corresponds to the difference between GB and FS segregation energies, is also calculated and compared with the previous theoretical results in detail.

The Ni Σ5 (012) GB is a typical tilt symmetrical grain boundary for face-centred-cubic (fcc) metals. In fcc structure, the vacancy site where small atoms can be inserted is an octahedral site. It is interesting to see how non-transition elements, having various atomic radii and electronegativities, can be different from each other in bonding character and stability in the GB, FS, and inner bulk sites of Ni. For example, a large mismatch in atomic size should cause a large strain energy in the Ni lattice, and the difference in electronegativity between Ni and the solute atom may reduce the covalency of the chemical bonding between them. These properties will affect the binding energy at the GB/FS/bulk sites and the embrittling potency energy.

2. Calculations

The first-principles electronic structure calculations in this study are based on the FLAPW method [2], which has been approved as one of the most accurate methods for the computation of the electronic structure of solids within density functional theory. In this method, the space in a crystal is divided into two regions: one is the muffin-tin (MT) sphere region which is centred at each nucleus, and the other is the interstitial region. In the MT sphere, the radial

part for both the electronic wavefunction and the charge density is expanded in numerical basis functions and the angular part in spherical harmonics. In the interstitial region, the electronic wavefunction and charge density are expanded in plane wave basis functions.

We used the WIEN2k code package [21, 22]. The cut-off parameters of the plane wave expansion are chosen to be $R(\mathrm{Ni})K_{\max} = 7$ for the wavefunction and $G_{\max} = 14$ for the charge density. The MT radius, R (atom), is set to be 0.7 au for H, 0.9 au for He, 1.1 au for the second row (from Li to Ne), 1.7 au for the third row (from Na to Ar), 1.95 au for the fourth row (from K to Kr), 2.1 au for the fifth row (from Rb to Xe), and 2.2 au for the sixth row (from Cs to Rn). The exchange–correlation functional is chosen to be GGA(PBE96) [23]. The energy of separation between the core and semicore is -8 Ryd. The Ni 3s state is treated as a core state and the 3p state as a semicore state. The local orbital for the Ni 3p state is included. For the valence states (e.g. Ni: 4s, 4p, 3d), the APW basis is used according to the default settings of WIEN2k. Almost all the calculations are carried out for the non-spin-polarized state. (For H, B, P cases, we performed both spin-polarized and non-spin-polarized calculations for comparison with the previous theoretical results.)

The unit cell structure is shown in figure 1. For the GB system, there are 20 Ni atoms (layers) and two GB layers in the unit cell. For the FS system, the same unit cell as for the GB is used, but the half of the crystal slab in the GB unit cell is removed. The length of the vacuum region is about 15 au. We took the non-symmetrical axes as $a = 6.62$ au in the $\langle 100 \rangle$ direction, $b = 8.11$ au in the $\langle \bar{1}2\bar{1} \rangle$ direction, and $\gamma = 114.094\,842^{\circ}$, where axes a and b are both on the GB/FS plane and perpendicular to the c axis. The length of the a axis (6.62 au) is the theoretical lattice constant that was determined in the case of fcc Ni using $R(\mathrm{Ni})K_{\max} = 7$ and $14 \times 14 \times 14$ k-points as stated in our previous paper [11]. The length of the c axis in the $\langle 012 \rangle$ direction is optimized. The k-point meshes are taken to be $4 \times 4 \times 1$.

In the total energy minimization procedure, it is necessary to circumvent time-consuming calculation when optimizing the atomic positions involving multilayer relaxation of the GB/FS in the presence/absence of the solute. For this reason, we set some restrictions on the displacement directions of the atoms and the flexibility of the unit cell in a way that is physically reasonable for most cases. The geometry optimization (the relaxation of the atomic positions) is done by force minimization using a damped Newton scheme for both the GB and FS systems. The geometry is optimized only along the c axis (parallel to the z coordinate, perpendicular to the GB/FS plane) for all the Ni and solute atoms except for the hydrogen (H) case. First, the geometry is optimized in a fixed unit cell. Next, for the GB systems, the length of the unit cell along the c axis is optimized by total energy minimization. Then, a set comprising a geometry optimization and a cell length optimization is performed once or twice more until the force tolerance of 2 mRyd au^{-1} is reached. In our experience, the second or third geometry optimization gives a reduction of only 1–2 mRyd/uc (0.01–0.03 eV/uc) in the total energy for all cases. As an exceptional case, in the Ni–H system, the position of the H atom is optimized in full space including x and y directions, as has been described in detail in our previous paper [11]. Another exceptional case is in the Ni FS–rare gas systems, since when the rare gas elements are on the FS, they are gradually moved away from the surface by force minimization. This means that rare gases are not able to bind to the Ni FS (or else, rare gases have extremely small energies of binding with the Ni FS). To confirm this, we set the rare gas elements about 5 au above the Ni surface, where they are settled by the geometry optimization. Then, the calculated binding energies were indeed very close to zero (this is seen later in figure 4).

The lengths of the a and b axes and the x and y coordinates of all the atoms are kept fixed to the values for bulk Ni. The forces acting on Ni atoms in the x and y directions (parallel to the GB/FS plane) are so small that the geometry optimization in these directions seems to be insignificant even when the solutes are placed in the GB sites. In fact, the GB calculations

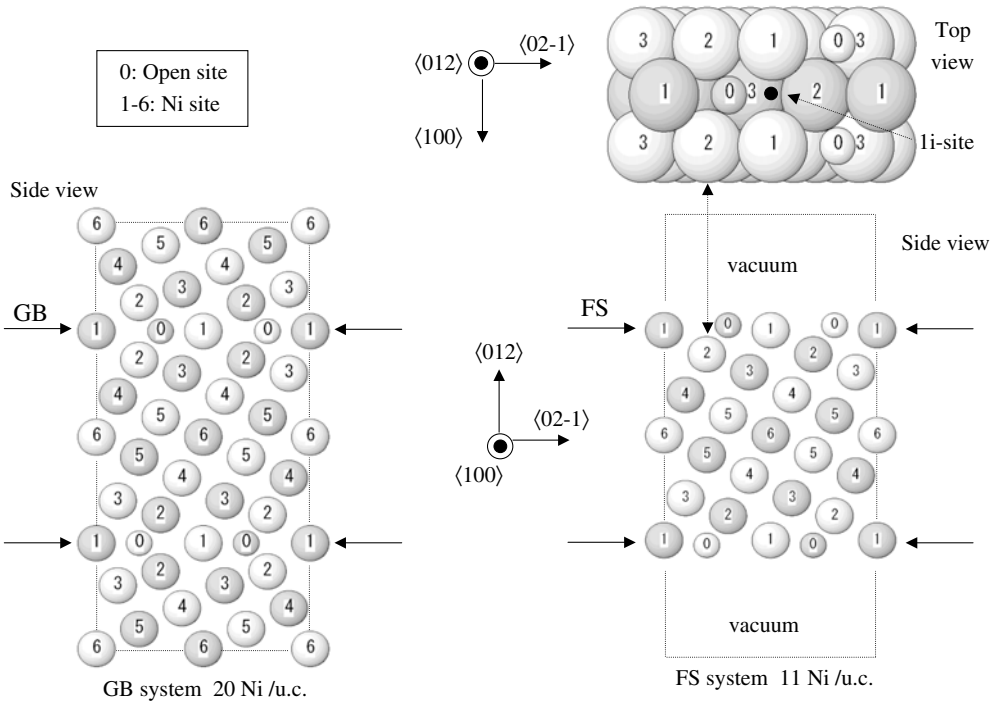

Figure 1. The unit cell structure for Σ5 (012) GB and (012) FS systems. The three directions ⟨100⟩, ⟨012⟩, and $\langle 02\bar{1}\rangle$ are shown by arrows. The ⟨012⟩ direction is parallel to the *c* axis, whose length is optimized for the GB system. For the GB system, a side view of the unit cell is shown. The unit cell includes 20 Ni atoms (layers). Each number indicates an equivalent site. The 0 site is an open space in the GB system. The layer that includes both the 0 site and the 1 site corresponds to the GB layer. For the FS system, a side view and a top view are shown. The unit cell includes 11 Ni atoms (layers) and a vacuum region. The Ni atoms in dark spheres are shifted by 0.5 *a* from the Ni atoms in white spheres in the ⟨100⟩ direction.

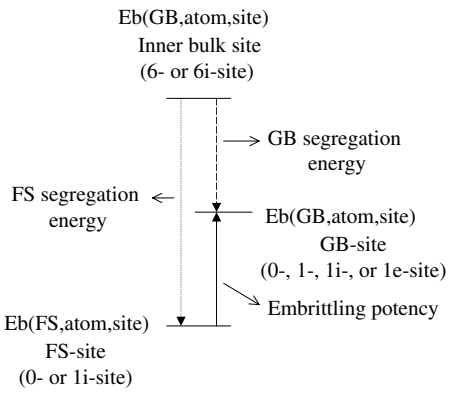

Figure 2. A schematic illustration of the relation among the binding energies of the solute atom. See the text.

done by other groups have also employed fixed *a* and *b* axes and fixed *x* and *y* coordinates. The only important difference between the present boundary conditions and those of earlier works [4–10] is that three-dimensional periodic boundary conditions are used. With these conditions, there are grain boundary planes with the period of ten Ni layers in the *z* direction.

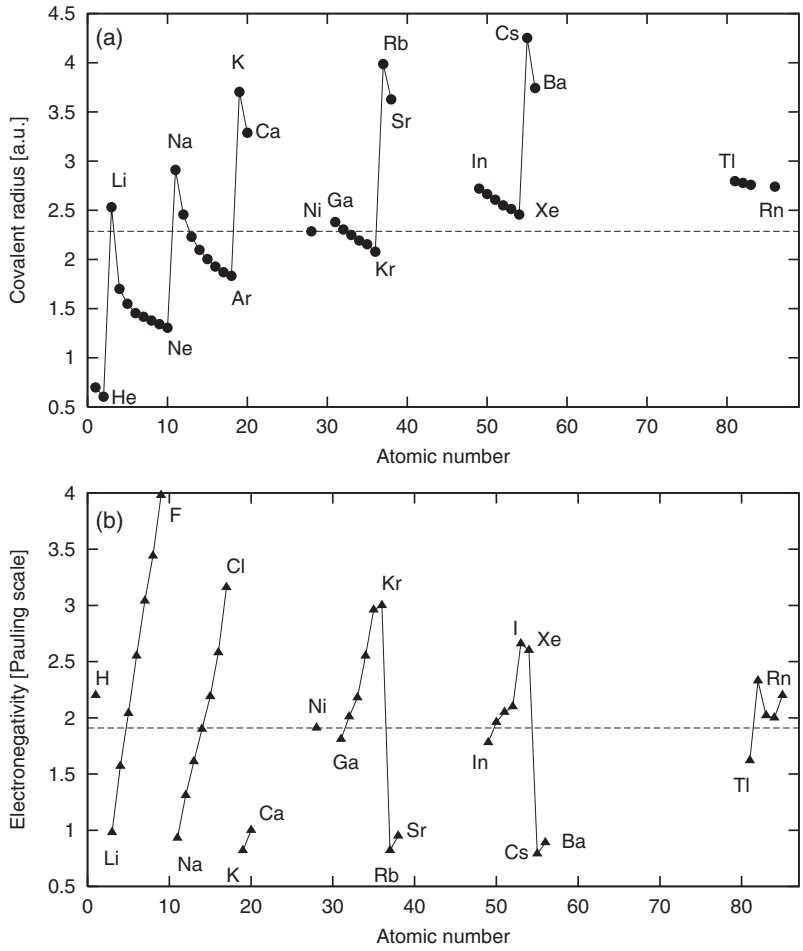

Figure 3. (a) The covalent radius (au) and (b) electronegativity (Pauling scale) for non-transition elements.

However, by some test calculations, it has been checked that the structure and energetics will not be altered significantly even when employing a larger unit cell. This means that the Ni lattice distortion due to the GB is concentrated near the GB plane so the interaction between the GB is negligible in the present case. The two crystals that meet at the GB are not allowed to translate parallel to the GB in our calculations while optimizing the geometry.

The GB/FS energy is evaluated using

$$\gamma(\mathrm{GB}) = \{E_{\mathrm{tot}}(\mathrm{GB}) - E_{\mathrm{tot}}(\text{bulk Ni})\}/2S \tag{1}$$

$$\gamma(\mathrm{FS}) = \{E_{\mathrm{tot}}(\mathrm{FS}) - \tfrac{11}{20}E_{\mathrm{tot}}(\text{bulk Ni})\}/2S \tag{2}$$

where $E_{\mathrm{tot}}(\mathrm{GB/FS})$ and $E_{\mathrm{tot}}(\text{bulk Ni})$ are (inherently negative) total energies for the GB/FS and bulk systems, respectively, and S is the interface/surface area of the GB/FS in the unit cell. The division by 2 means that two GB/FS interfaces are included in a unit cell. First-principles calculation of $E_{\mathrm{tot}}(\text{bulk Ni})$ has been carried out under the same conditions as for the GB/FS system except that Ni is arranged in the fcc structure; the unit cell contains 20 Ni atoms, and 20 atomic layers are repeated periodically in the $\langle 012 \rangle$ direction in the fcc arrangement. Again,

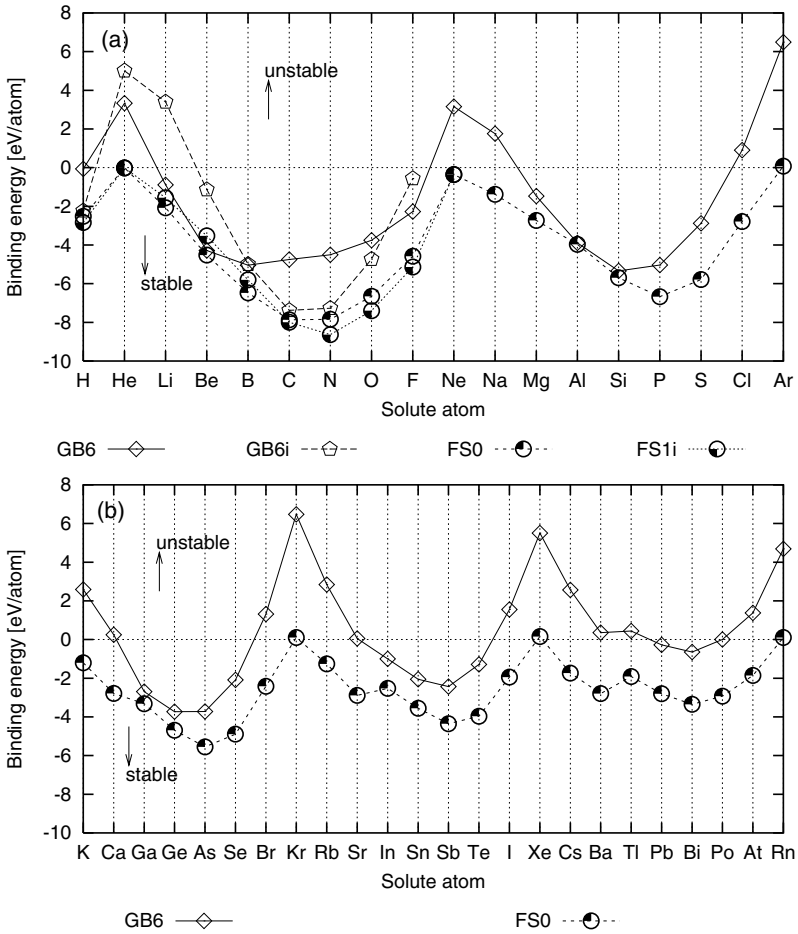

Figure 4. Calculated binding energies of solute atoms at different sites. In our definition, negative binding energy means stable. (a) For inner bulk sites (GB6, GB6i) and FS sites (FS0, FS1i) from H to Ar. (b) For inner bulk sites and FS sites from K to Rn. (c) For GB sites (GB0, GB1, GB1e, GB1i) from H to Ar. (d) For GB sites from K to Rn.

the length of the c axis is optimized by total energy minimization. Using an identical or almost the same unit cell is technically important for an accurate calculation of the energy difference of the two structures, since the electronic structure calculation should be performed using the same calculation parameters (MT radius, number of k-points, $RK_{\max}$, etc).

In figure 1, we show several different positions of the solute atoms considered in our calculations. For the GB system, a solute atom is placed either at a 0 site, 1 site, 1e site, 1i site, 6 site, or 6i site. The 0 site is located in an open space on the GB plane (the first Ni layer). The x and y coordinates of this site correspond to those of Ni atoms in the layer subsequent to the first layer on the opposite side of the second layer for the bulk system. The 1 site indicates the case of substitution of the Ni atom in the first layer with the solute atom. The 1e site means the situation where the solute atom occupies the 1 site and the Ni atom occupies the 0 site. In other words, the 1e site configuration is realized by exchanging the first Ni layer atom and the solute atom in the 0 site configuration. The 1i site corresponds to an octahedral site in the fcc lattice which is located on the GB plane. The 1i site on the GB plane is found to be a stable site

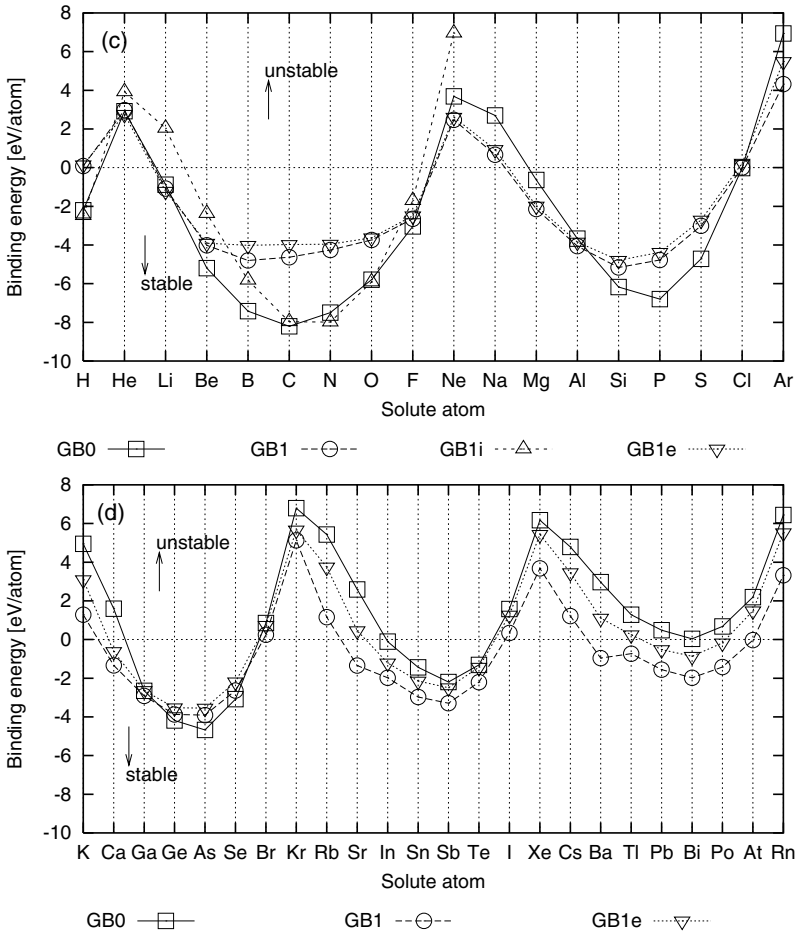

Figure 4. (Continued.)

for hydrogen as shown in the previous paper [11]. The 6 site indicates the case of substitution for the sixth-layer Ni atom of the solute. Since the sixth layer is little affected by the grain boundary, we regard the 6 site as the substitutional inner bulk site. In fact, we confirmed that the calculated binding energies of phosphorus at the 6 site in the GB system unit cell and at an appropriate site in the bulk system unit cell as stated above are not significantly different. The 6i site is an octahedral site which is in the interstitial space on the same plane as the sixth Ni layer. This site is regarded as the interstitial site in bulk Ni. For the FS system, a solute atom is placed either at the 0 site or the 1i site, similarly to in the definitions mentioned above.

The binding energy of the solute atom is calculated using

$$E_{\mathrm{b}}(\mathrm{GB/FS, atom, site}) = \{E_{\mathrm{tot}}(\mathrm{GB/FS, atom, site}) - E_{\mathrm{tot}}(\mathrm{GB/FS}) - E_{\mathrm{tot}}(\mathrm{atom})\}/2 \qquad (3)$$

where $E_{\mathrm{tot}}(\mathrm{GB/FS, atom, site})$, $E_{\mathrm{tot}}(\mathrm{GB/FS})$, and $E_{\mathrm{tot}}(\mathrm{atom})$ are the total energies of the GB/FS system with a solute depending on the binding site, the GB/FS system without a solute, and an isolated solute atom, respectively, which are evaluated by independent first-principles calculation runs. In the case of the substitutional 1 site and 6 site, $E_{\mathrm{tot}}(\mathrm{bulk\ Ni})/10$ is subtracted from $E_{\mathrm{tot}}(\mathrm{GB})$, considering that two Ni atoms are taken away from the unit cell.

In this definition, a large value with a negative sign means that the solute atom makes strong bonds and is stable in the host Ni metal. In all these total energy calculations except for the case of an isolated hydrogen atom ($E_{\rm tot}$(H)), we used the same type of unit cell, excluding in the geometry optimization and cell optimization along the c axis, and set the calculation parameters as the same in order to calculate the total energy differences accurately. We note that a set comprising a geometry optimization and a cell optimization is done independently for each kind of solute and each binding site. Only for $E_{\rm tot}$(H) did we use the supercell of the fcc structure that had the 20 au lattice constant with R(Ni)$K_{\rm max} = 7$ and one k-point in order to make a more precise comparison of the GB/FS binding energies between our calculations and experiments.

The energy diagram for the GB/FS segregation energy and embrittling potency energy is shown schematically in figure 2. The GB/FS segregation energy, $E_{\rm seg}$(GB/FS, atom), is defined as the binding energy difference between the most stable (minimum total energy) site at the inner bulk (6 or 6i site) and at the GB/FS (0-, 1-, 1e-, or 1i site at the GB/0 or 1i site at the FS) depending on the atomic element:

(inner)bulk-site : GB6, GB6i

GB-site : GB0, GB1, GB1e, GB1i

FS-site : FS0, FS1i

$$E_{\rm seg}({\rm GB, atom}) = \min\{E_{\rm b}({\rm GB, atom, GB\text{-}site})\} - \min\{E_{\rm b}({\rm GB, atom, bulk\text{-}site})\} \quad (4)$$

$$E_{\rm seg}({\rm FS, atom}) = \min\{E_{\rm b}({\rm FS, atom, FS\text{-}site})\} - \min\{E_{\rm b}({\rm GB, atom, bulk\text{-}site})\}. \quad (5)$$

A large value with a negative sign means that the solute atom is stable at the segregated site.

The embrittling potency energy $\Delta E_{\rm b}$(atom), which is related to the Rice–Wang model [3], is defined as the difference between the GB and FS segregation energies depending on the atomic element or as the difference in binding energies between the most stable GB site and FS site:

$$\Delta E_{\rm b}({\rm atom}) = E_{\rm seg}({\rm GB, atom}) - E_{\rm seg}({\rm FS, atom}) \quad (6)$$

$$= \min\{E_{\rm b}({\rm GB, atom, GB\text{-}site})\} - \min\{E_{\rm b}({\rm GB, atom, FS\text{-}site})\}. \quad (7)$$

A positive/negative value of $\Delta E_{\rm b}$ means that the solute atom has an embrittling/strengthening effect on the GB. Note that the segregation and embrittling potency energies are not affected by the value of $E_{\rm tot}$(atom) since they are only related to the difference of the binding energies.

3. Results and discussion

3.1. General trends for all the non-transition elements

We first made calculations for the clean Ni GB and FS systems without solute atoms. The GB and FS energies for the non-magnetic (magnetic) state were 1.41(1.43) and 2.64(2.65) J m^{-2}, respectively, corresponding to 1.21 and 2.27 eV/atom at the GB and FS, respectively. The work function in the FS system was 4.65 eV. By test calculations in a larger unit cell (28 atom/uc for the GB and 15 atom/uc for the FS), we confirmed that these values did not change significantly. As has been also shown in our previous paper [11], the calculated interlayer distances are in good agreement with the other first-principles calculations by Geng *et al* [9]. It is worthwhile to note that the three-dimensional boundary condition in the WIEN2k code seems not to be harmful in the present case, since our results agree well with those in the two-dimensional film code [9].

As a preparation for the discussion below, we show the series for the covalent radius [24–29] and Pauling electronegativity [26–31] of the non-transition elements in figures 3(a) and (b),

respectively. The data on Ni are also shown for comparison. As a general trend, the covalent radius decreases from left to right in the same row, and increases from top to bottom in the same column in the periodic table. On the other hand, the electronegativity increases from left to right, and decreases from top to bottom. Now, Hume-Rothery's rule is as follows:

(1) if a solute differs in its atomic size by more than about 14% from the host, then it is likely to have a low solubility in that metal;
(2) if a solute has a large difference in electronegativity when compared with the host, then it is more likely to form a compound—its solubility in the host would therefore be limited;
(3) a metal with a higher valency is more likely to dissolve in one which has a lower valency, but not vice versa.

Figures 4(a) and (b) show the calculated binding energies of solute atoms at the substitutional site in the inner bulk (GB6) and at the surface site (FS0). For light elements from H to F, the solute binding energies at the interstitial sites in the inner bulk (GB6i) and at the interstitial surface site (FS1i) are also shown. Although the interstitial binding energies were not explicitly calculated for the heavier elements, their atomic radii are obviously too large for them to be stable at the interstitial sites. Because of our restriction in computational time, the position of the solute atom on the FS has been limited to FS0 and FS1i sites instead of a three-dimensional global search being performed. In our definition, a negative binding energy means that the solute atom is stable. From these figures, we can find the following characteristics:

(1) As a general trend, the solute binding energies at the bulk and FS show an oscillatory behaviour across the periodic table. The elements that are around the middle part in the periodic table are more stable than those around both edge parts such as rare gases, halogens, and alkali metals. This means that the covalent bonding between Ni and the solute atoms plays an important role, and Hume-Rothery's rule No 2 works qualitatively; the bonding is tight when the electronegativity is similar between Ni and the solute, as we can see by comparing figure 4 with figure 3(b). The binding energy curve becomes shallower from light elements to heavy elements. This is affected by Hume-Rothery's rule No 1, since heavy elements have larger radii than Ni as shown in figure 3(a).
(2) For most of the elements, the lowest energy (most stable) position for the solute in the bulk is the substitutional site, GB6. However, as exceptions, the solutes H, C, N, and O are more stable in the interstitial site, GB6i, in the bulk. Boron has almost the same binding energy at the interstitial and substitutional sites. This is consistent with experimental observations that these elements behave as interstitial atoms in metals. Also at the FS, elements such as H, C, N, O, and F prefer the interstitial site, FS1i, while all the other elements prefer the substitutional site, FS0.
(3) Rare gases (He, Ne, Ar, Kr, Xe, Rn) and alkali metals (Na, K, Rb, Cs) and some halogens (Cl, Br, I, At) have positive and large binding energy in the bulk. This means these elements are not easy to dissolve in bulk Ni.
(4) For rare gases (He, Ne, Ar, Kr, Xe, Rn), the binding energies are almost zero on the FS. This means that rare gases may not create chemical bonds with the Ni surface.

It should be noted here that all the binding energies in figure 4 are calculated in the non-spin-polarized state (except for the H case) to reveal a general trend and allow comparison of these results with each other, systematically, under the same conditions. For this reason, even the isolated atoms that have a large magnetic energy are also treated in the non-spin-polarized state. For example, the isolated oxygen atom has a large magnetic energy, which is the reason for making the binding energy of oxygen very large in our calculations. The total energy of

an isolated oxygen atom in the triplet state is lower than that in the singlet state by 1.47 eV/O in our calculation. Using this value (1.47 eV/O) and the binding energy of the O_2 molecule (5.87 eV/O_2) calculated by Eichler *et al* [32], the dissociative adsorption energy of the O_2 molecule is calculated to be −2.25 eV/O at the FS0 site and −2.99 eV/O at the FS1i site per half an O_2 molecule. These values did not change significantly when we calculated for the spin-polarized state. The former value is in good agreement with the calculated result (−2.32 eV) obtained by Eichler *et al* [32] and the experimental value (−2.28 eV) for an adsorbed oxygen atom at a fcc hollow site on a Ni(111) surface. It is interesting that the latter value is much lower than the former value. The dependence of the binding energy on the binding site should be investigated in more detail since it affects the final segregation energy and embrittling potency energy. However, we restrict the binding sites to save computational time. One of our main purposes in this paper is to reveal general trends for many elements.

Figures 4(c) and (d) show the calculated binding energies at the GB sites. The following features can be seen in these figures.

(1) The oscillatory behaviour across the periodic table is qualitatively similar to that of the bulk binding energy. The rare gases, alkali metals, and some halogens are stable at neither of the GB sites.
(2) H, N, and O atoms are most stable at the GB1i site because of their small atomic radii. The GB0 site is also stable for these elements.
(3) He and Li atoms are most stable at the GB1e site. They are also stable at the GB0 and GB1 sites.
(4) The elements in the middle part of the second–fourth rows (Be, B, C, F, Si, P, S, Cl, Ge, As, Se) are most stable at the GB0 site.
(5) Other elements, in both edges of the second–fourth rows and in the fifth and sixth rows, are most stable at the GB1 site because of their large atomic radii.

Figures 5(a) and (b) show the calculated interlayer distances of Ni atoms in the GB configuration when various solute atoms are placed at the GB0 site. Similar figures for the FS configuration are given in figures 6(a) and (b). In these figures, the lattice expansion due to the insertion of a solute atom at the GB (FS) is characterized by the interlayer distance between the GB6 (FS6) and GB0 (FS1) layers. The extent of lattice expansion may be analysed from the atomic radius and ionicity of the solute. For instance, in the second-row elements, we can see that the lattice expansion slightly decreases from Li to N and increases from N to Ne, whereas the covalent radius decreases monotonically from Li to Ne as shown in figure 3(a). The increase in the lattice expansion from N to F can be ascribed to the ionic bonding between Ni and the solute. This is because these solute atoms have larger electronegativity than Ni and become anions, as can be seen in figure 3(b), and accordingly the Ni lattice is expanded by those anions having large ionic radii. A large lattice expansion seen in Ne may be due to the repulsive character of the interaction between rare gas and Ni. As a result, the elements in the middle part of the row have the smallest lattice expansion of the GB. This trend is also seen in the third–sixth-row elements. The lattice expansion becomes larger for heavier solutes, as can be expected from their atomic radii. It is interesting to note that most of the lattice distortion is generally concentrated in the interface layers GB1, GB2 and surface layers FS1, FS2.

Figures 7(a) and (b) show the calculated segregation energies at the GB and FS for each solute atom. From these figures, we find the following trends.

(1) For most non-transition elements, the FS/GB segregation energies are appreciably negative. This means that all kinds of solutes within non-transition elements are more stable in the FS/GB than in the bulk.

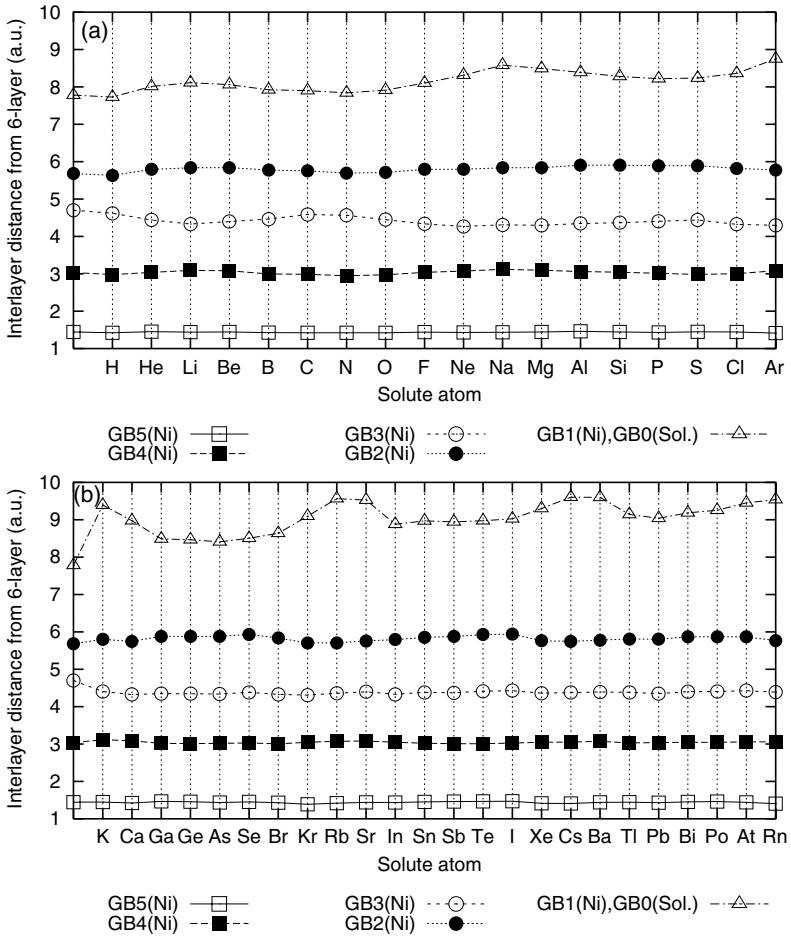

Figure 5. Distances (au) of each Ni layer from the GB6 layer in the GB system with a solute atom at the GB0 site. The result for a clean Ni grain boundary is shown on the left. (a) From H to Ar. (b) From K to Rn.

(2) Since the light elements in the first and second rows are bound to various interstitial or substitutional sites at the bulk and GB depending on the solute, the FS and GB segregation energy curves show somewhat complex behaviour. Meanwhile, the segregation energies in the third–sixth rows show clean oscillatory behaviour, as the solute occupies only the bulk/GB substitutional sites.

(3) The GB segregation energies vary from 0 to about $-2.5\,\mathrm{eV/atom}$, while the FS segregation energies vary from 0 to about $-6.5\ \mathrm{eV/atom}$. Several solutes that have the largest (negative) GB segregation energies are B, P, S, and some rare gas elements (Ar, Kr, Xe). The solutes that have largest (negative) FS segregation energies are found in the heavy elements among the rare gases (Ar, Kr, Xe, Rn), alkali metals (K, Rb, Cs), and halogens (Cl, Br). Here, the FS segregation energies of the rare gases are almost the same, with the negative sign, as their bulk binding energies, since they have only small energies of binding with the FS. Thus, 'FS segregation' might not be an appropriate term for the rare gases in a rigorous sense.

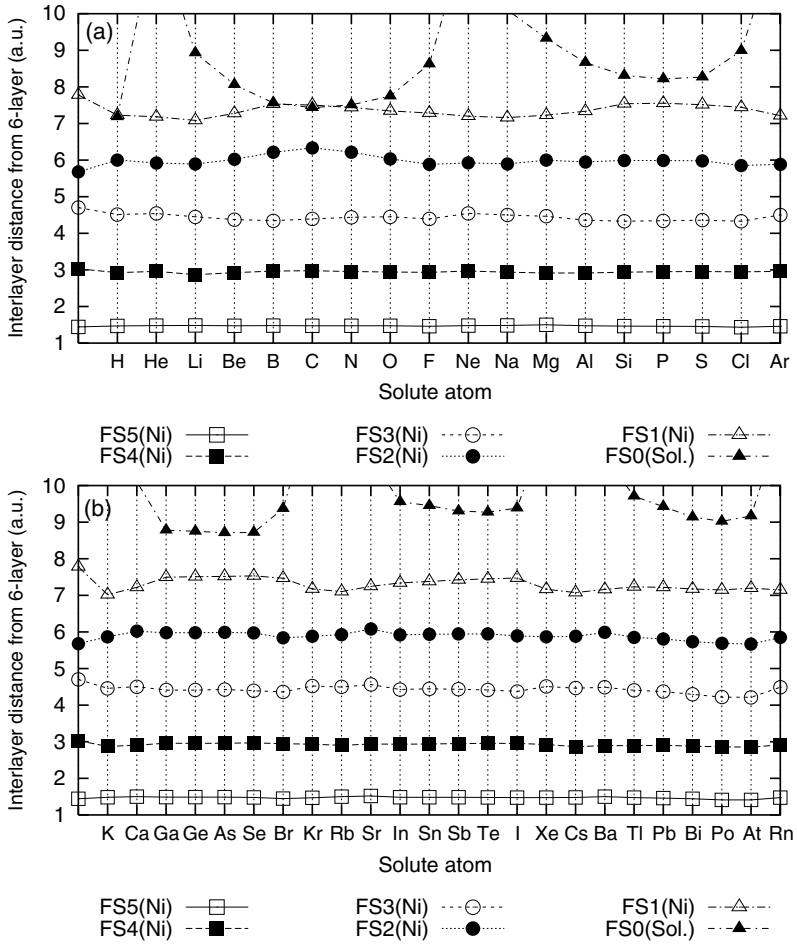

Figure 6. Distances (au) of each Ni layer from the FS6 layer in the FS system with a solute atom at the FS0 site. The result for clean Ni surface is shown on the left. (a) From H to Ar. (b) From K to Rn.

Finally, we show the calculated embrittling potency energies in figures 8(a) and (b). We can see the following features from these figures.

(1) A clear oscillatory behaviour is seen throughout the periodic table for first–sixth elements. The embrittling potency energies are positive for most of the solute elements.
(2) Some solutes which have negative embrittling potencies are Be, B, C, Al, Si, and P. In particular, Be, B, C, and Si have appreciable negative values for the embrittling potencies. This means that these elements are GB cohesion enhancers. The elements Al and P have close to zero embrittling potencies.
(3) The embrittling potencies are largest in rare gases, alkali metals, and halogens.

Here, we would like to make a brief comment on an extreme behaviour of rare gases. Experimentally, helium air bubbles, which are generated by nuclear fission reaction of B, Be, and Li atoms embedded in the solid, cause strong embrittlement. This phenomenon is well known as ‘fission gas swelling’. We can see that this is consistent with our calculated results

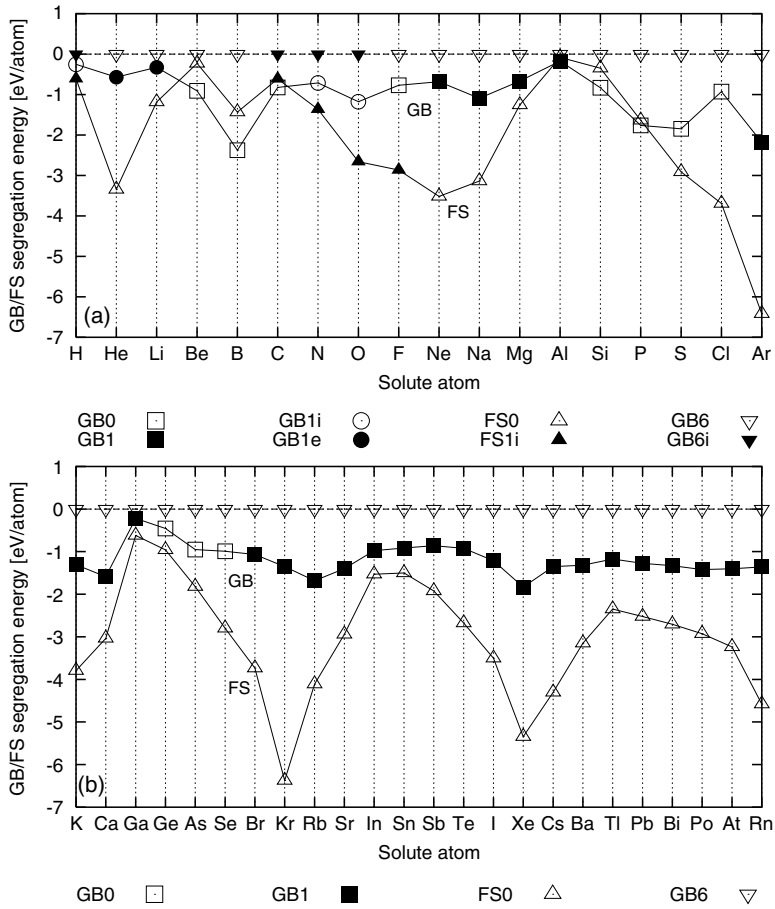

Figure 7. Calculated GB/FS segregation energy for solute atoms. As shown in figure 2, this is the difference in binding energy between the most stable inner bulk site and the GB/FS site, which are indicated by symbols. The origin (zero) of the energy is set to the binding energy at the most stable inner bulk site (GB6 or GB6i). (a) From H to Ar. (b) From K to Rn.

for rare gases. In our results, the He atom has the almost zero binding energy on the FS as shown in figure 4(a). (To be precise, the He atom tends to go away from the Ni surface upon geometry optimization.) In addition, the binding energies at the inner bulk sites (GB6, GB6i) as well as the GB sites (GB0, GB1, GB1i, GB1e) show positive and large values as shown in figure 4(c) indicating that He atom is highly unstable inside Ni. Comparing the two binding energies at the most stable GB site (GB1e) and the inner bulk site (GB6), this energy at the GB1e site is appreciably lower than that at the inner bulk site as shown in figure 7(a), which means that He can segregate to the GB. As a result, the appreciable size of the GB segregation energy (-0.61 eV/He) and the extremely large embrittling potency energy (2.78 eV/He) are obtained in our results. This trend is the same for all the other rare gas elements.

3.2. Comparison with experiments: GB/FS segregation energies

Now, it is interesting to compare our calculated data with experimental and theoretical results in the literature. Tables 1 and 2 summarize the comparison between our calculated segregation

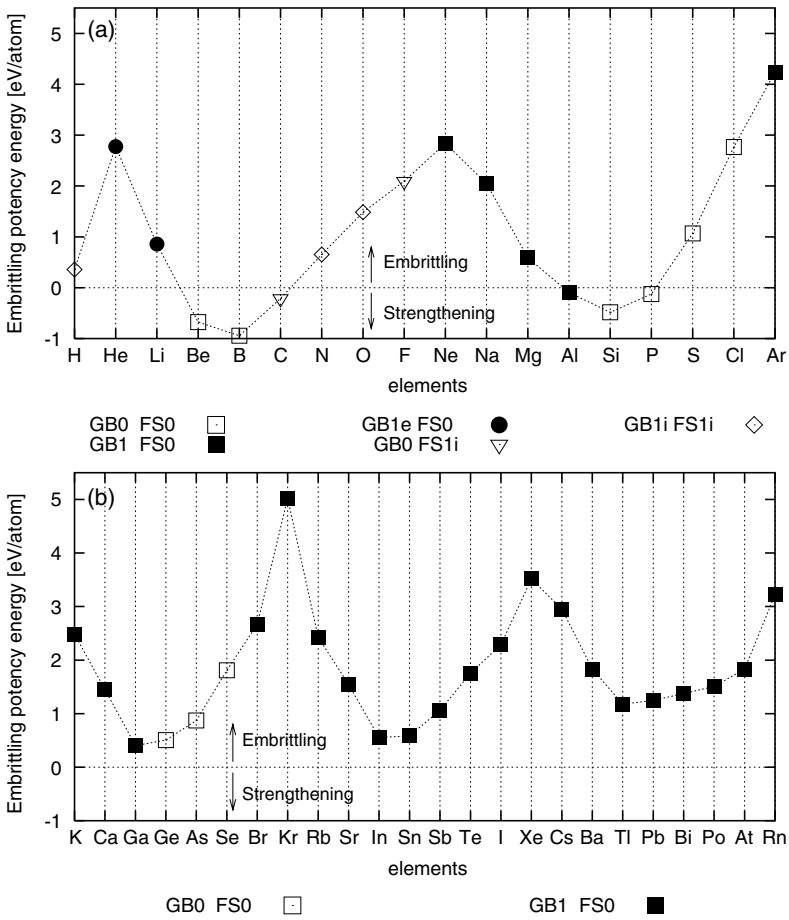

Figure 8. Calculated embrittling potency energy (eV/atom) for solute atoms. This is the difference between the GB and FS segregation energies as shown in figure 2. This is calculated using the most stable GB and FS sites, which are indicated by symbols. (a) From H to Ar. (b) From K to Rn.

energy and the experimental enthalpy (Δh) and/or free energy ($\Delta g = \Delta h - T\Delta s$; Δs: entropy term) of segregation determined from the analysis of (mostly) Auger electron spectroscopy for some solute elements. Here, we mention briefly the entropy terms that are not shown in these tables. Rice and Wang [3] estimated that the typical entropy term (Δs) was about 0.01–0.03 kJ mol^{-1} for GBs and 0–0.03 kJ mol^{-1} for FSs from some experimental data. According to them, the free energy ($-\Delta g$) is larger than the enthalpy ($-\Delta h$) by about 0–30 kJ mol^{-1} at 1000 K depending on the solute elements and the experimental circumstances.

First, the energetics of the H atom in Ni can be compared quantitatively. In our previous paper [11], we have already shown that our calculated binding energies are in excellent agreement with the experimental adsorption energy of the H atom on a Ni(111) surface and the energy of absorption in bulk Ni. Experimentally, the GB segregation enthalpy of hydrogen was estimated to be -11.6 kJ mol^{-1} (-0.12 eV/H) [34], based on the fracture mode dependence on the bulk hydrogen concentration and ageing temperature. Our calculated GB segregation energy for the spin-polarized state is -0.31 eV/H (-30 kJ mol^{-1}). The difference of these values might come from the definition of the segregated region of H. The

Table 1. The calculated and experimental GB/FS segregation energies (kJ mol^{-1}) for H, B, C, P, and S in the non-spin-polarized state except for the H case. Δh denotes the enthalpy of segregation. Δg (at T) denotes the free energy of segregation (with temperature). (1 eV/particle = 96.53 kJ mol^{-1}.)

Sol.	C/E	Sample	GB/FS	$-\Delta h$	$-\Delta g$ (at T)	References
H	Cal.	Ni	Σ5 (012)GB	30(0.31 eV)	—	This work
	Exp.	Ni	GB	11.6	—	Lassila [34]
	Cal.	Ni	(012)FS	69(0.71 eV)	—	This work
			(111)FS	69	—	This work
	Exp.		(111)FS	55–66	—	See text
B	Cal.	Ni	Σ5 (012)GB	229(2.37 eV)	—	This work
	Exp.	Fe[a]	GB		100(1073 K)	Liu [53]
	Cal.	Ni	(012)FS	138(1.43 eV)	—	This work
C	Cal.	Ni	Σ5 (012)GB	80(0.83 eV)	—	This work
	Exp.	Fe[a]	GB		80(1073 K)	Suzuki [54]
		Fe	GB	57	—	Grabke [55][d]
		Fe	GB	79[b]	—	Papazian [56][d]
	Cal.	Ni	(012)FS	59(0.61 eV)	—	This work
	Exp.	Ni	(111)FS	53	—	Shelton [57]
		Fe	(100)FS	85	—	Grabke [55][d]
P	Cal.	Ni	Σ5 (012)GB	170(1.76 eV)	—	This work
	Exp.	NiCrFe[c]	GB	—	40.8(700 °C)	Was [58]
		NiCrFe[c]	GB	—	46.2(1100 °C)	Was [58]
		Fe[a]	GB	—	50(1073 K)	Suzuki [54]
		Fe	GB	34	—	Grabke [55][d]
	Cal.	Ni	(012)FS	157(1.63 eV)	—	This work
	Exp.	Ni	(poly)FS	—	89(1048 K)	Zhang [48]
		Fe	(low)FS	180	—	Grabke [59][d]
		Fe	(poly)FS	—	>80(973 K)	Guttmann [60][d]
		Fe	(poly)FS	75	—	Grabke [55][d]
S	Cal.	Ni	Σ5 (012)GB	179(1.85 eV)	—	This work
	Exp.	Ni	GB	—	98(700 °C)	Larere [43]
		Fe[a]	GB	—	75(1143 K)	Suzuki [61][d]
	Cal.	Ni	(012)FS	281(2.91 eV)	—	This work
	Exp.	Ni	(low)FS	180	—	Qudar [62]
		Ni	(poly)FS	—	123(1048 K)	Zhang [48]
		Ni	(poly)FS	135		Miyahara [47]
		Fe	(poly)FS	190	—	Grabke [55][d]

[a] High purity iron.
[b] Autoradiography data.
[c] Ni–16Cr–9Fe.
[d] Summarized in Rice–Wang's report [3].

value observed experimentally is the mean value for H atoms segregated in polycrystalline Ni GBs, which are found to be widely spread within a range of about 35 nm from the GB plane. Meanwhile, our calculation treats the segregation energy of the primary site (the 1i site) on the Σ5 (012) GB plane. Although we did not calculate the H segregation energies on the secondary trapping sites on both sides of the GB, they should gradually become close to zero on approaching the bulk site. It is for the above reason that the calculated GB segregation energy is a rather larger value, with a negative sign, than the experimental one. On the other hand, the experimental FS segregation energy is estimated to be −55 to −66 kJ mol^{-1}, which is taken from the difference between the adsorption energy (−2.87 eV/H [35], −2.90 eV/H [36]) of

Table 2. The same as table 1, but for N, O, Si, In, Sn, and Sb.

Solute	C/E	Sample	GB/FS	$-\Delta h$	$-\Delta g$ (at T)	References
N	Cal.	Ni	Σ5 (012)GB	69(0.71 eV)		This work
	Cal.	Ni	(012)FS	132(1.37 eV)		This work
	Exp.	Fe	(100)FS	110		Grabke [55]
O	Cal.	Ni	Σ5 (012)GB	114(1.18 eV)		This work
	Cal.	Ni	(012)FS	257(2.66 eV)		This work
Si	Cal.	Ni	Σ5 (012)GB	80(0.83 eV)		This work
	Cal.	Ni	(012)FS	34(0.35 eV)		This work
	Exp.	Fe	(100)FS	48		Grabke [55]
In	Cal.	Ni	Σ5 (012)GB	94(0.97 eV)		This work
	Exp.	Ni	GB		33–50(970 K)	Muschik [63]
	Cal.	Ni	(012)FS	148(1.53 eV)		This work
Sn	Cal.	Ni	Σ5 (012)GB	88(0.91 eV)		This work
	Exp.	Fe	GB	23		Grabke [59][b]
		Fe	GB	13	45(823 K)	Seah [64][b]
	Cal.	Ni	(012)FS	145(1.50 eV)		This work
	Exp.	Fe	(low)FS	>200		Grabke [59][b]
		Fe	(poly)FS	46	77(823 K)	Seah [64][b]
Sb	Cal.	Ni	Σ5 (012)GB	83(0.86 eV)		This work
	Exp.	Fe	GB		20–40(1023 K)	Guttmann [65][b]
		Fe	GB	13[a]		Guttmann [66][b]
	Cal.	Ni	(012)FS	185(1.92 eV)		This work
	Exp.	Fe	(poly)FS		>105(1023 K)	Dumoulin [67][b]

[a] Rutherford back scattering spectroscopy data.
[b] Summarized in Rice–Wang's report [3].

H on the Ni(111) surface and the absorption energy (−2.30 eV/H [35], −2.22 eV/H [37]) in the inner bulk of Ni. Our calculated values for this FS segregation energy of H on the Ni(111) and Ni(012) surfaces give the same results of −0.71 eV/H (−69 kJ mol^{-1}), which are in good agreement with the experimental result for the Ni(111) surface. Also, in our previous semiempirical EAM calculations [12], the GB/FS segregation energies are about −0.3 eV for various symmetrical tilt GBs (Σ3 (111), Σ5 (012), Σ7 (132), Σ9 (221), ...) and about −0.6 eV on various FSs. From these results, the H segregation energies do not depend so much on the types of Ni GBs and FSs. This may be due to the Ni–H bonding character which is not sensitive to the bonding direction (in contrast to covalent bonding).

Next, the GB/FS segregation and embrittling potency energies are discussed at a qualitative level. There are several reasons for the difficulty of the comparison between theory and experiment. For our calculation, the segregation sites and inner bulk sites are limited to only a few sites due to the limitation of the size of the unit cell. In addition, we estimate the effect of lattice expansion and geometry optimization only in the direction of the c axis and not in the ab plane. Experimentally, on the other hand, measurements for the corresponding data have not been done in ideal conditions. The influences of the other impurity elements or other types of defects cannot be excluded as easily in experiments as in the calculations. Experimentally, the concentration of the segregant element at GB facets is observed by fracturing the specimen and then analysing using Auger electron spectroscopy. Then, the free energy and/or enthalpy of segregation are estimated from the temperature dependence of the segregant concentration based on the Langmuir–McLean model [38]. (The calculated segregation energy corresponds to the experimentally determined enthalpy of segregation, since the pressure times volume

term (pV) in the enthalpy is considered to be negligible under unstressed conditions.) The experimentally estimated segregation energy is an average value for many kinds of GBs that are not precisely known. In fact, Lejček *et al* [39] showed that the experimental GB segregation energies of C, Si, and P in α-Fe depended on the characteristics of grain boundaries. Similarly, the FS segregation energy might depend greatly on the characteristics of the surface in some cases. For example, the experimental FS segregation energies of P on a low index Fe surface and a polycrystalline surface differ about a factor of two as shown in table 1. In this way, the experimentally determined energies are greatly dependent on the detail of the experimental circumstances. Furthermore, there are no experimental data for pure Ni for some solute elements as far as we know. In such cases, we show the data for Ni alloy, pure Fe, and/or Fe alloy instead of pure Ni.

The comparisons for the solutes B, C, P, and S are also shown in table 1. For the B atom, there are no experimental data for segregation energies in Ni GB/FS as far as we know. However, B is well known to have the effect of causing recovery from intergranular hydrogen embrittlement (IGHE) for Ni [40, 41]. In addition, an experimental analysis suggests the following things [42]: B has the effect of strengthening the GBs and also reducing the embrittling effect of S segregation on GBs. From our calculated data, this could be explained by a simple scenario wherein B has (negative and) larger GB segregation energy than H (S), and B has negative embrittling potency. This means that the B atom can replace the segregated H (S) atom at the GBs via site competition, which will enhance the Ni GB cohesion. In fact, the calculated GB segregation energy of B (-229 kJ mol^{-1}) is larger than that of H (-30 kJ mol^{-1}), that of S (-179 kJ mol^{-1}), and the calculated FS segregation energy of B (-138 kJ mol^{-1}). This trend is also found in the experimental free energy of segregation for the case of B segregation in pure Fe GBs (-100 kJ mol^{-1} at 1073 K), which is a relatively large value compared with those for S (-75 kJ mol^{-1} at 1143 K). Furthermore, the above experiment [42] also suggests that B does not influence the FS segregation of S on the Ni surface. This means that the FS segregation energy of S is larger than that of B on the Ni surface, which is also consistent with our calculated results (S: -281 kJ mol^{-1}; B: -138 kJ mol^{-1}). However, it would be too early to give our final conclusion on this phenomenon at this stage since the interaction between B and H (S) atoms is not investigated here directly.

For C atoms, experimental data exist for Ni(111) FS. The experimental (111) FS segregation enthalpy is -53 kJ mol^{-1}, which is in good agreement with our calculated value for the (012) FS, -59 kJ mol^{-1}. For the GB segregation energy, the calculated value -80 kJ mol^{-1} is very similar to the experimental one in the Fe GB, ranging from -57 to -80 kJ mol^{-1}. Although there are no experimental data for the GB segregation energy of C in Ni, the experimental analyses suggest that the GB segregation energy of C in Ni must be smaller than that of S [43] and that C decreases the extent of the IGHE of Ni [44]. In our results, the GB segregation energy of C is -80 kJ mol^{-1}, which is smaller than that of S (-281 kJ mol^{-1}) and larger than that of H (-30 kJ mol^{-1}). These values are consistent with the above experimental facts.

For P atoms, there are experimental data for the FS segregation energies on the Ni surface and the GB segregation energy in Ni–16Cr–9Fe alloy. Both of these experiments gave somewhat smaller values than our calculation, but they are still of the same order of magnitude. However, we note that the experimental segregation enthalpy for P on a low index Fe surface (-180 kJ mol^{-1}) is much larger than that on the polycrystalline Fe surface (about -75 kJ mol^{-1}). Thus, the FS segregation energy of P on a Ni surface might also be dependent on the characteristics of the Ni surface, which should be investigated more. For S atoms, experimental data exist for both the GB and FS segregation energies in Ni. Like for P on an Fe surface, the FS segregation energy of S on a low index Ni surface is appreciably larger

than that on the polycrystalline surface. The calculated results are larger than the experimental ones, but they are still of the same order of magnitude.

Comparing the calculated GB/FS segregation energies for B, P, and S atoms with that for the C atom, the energies of B, P, and S are much larger than that of C and the corresponding experimental data. In the case of high purity Fe, the experimental GB segregation free energy (Δg) of C (-80 kJ mol^{-1}) is only a little smaller than that for B (-100 kJ mol^{-1}) and larger than those for P (-50 kJ mol^{-1}) and S (-75 kJ mol^{-1}). These experimental results seem to be inconsistent with our results for Ni. However, at this stage we do not know in detail about the difference in GB segregation between bcc Fe and fcc Ni.

The GB/FS segregation energy depends on the binding energies both in the inner bulk and at the GB/FS, since it is the energy difference between the two. Here, we give the FS segregation energy of S in detail, as an example. The calculated bulk binding energy of S in Ni is -2.49 (-2.88) eV/atom with respect to an isolated S atom in the triplet (singlet) state, which is smaller by about 1.0 eV/atom comparing with the experimental value -3.5 eV/atom [47], while the calculated binding energy of S on the Ni(012) surface is -5.40 (-5.79) eV/atom with respect to an isolated S atom in the triplet (singlet) state, which is about 0.49 eV larger than the experimental binding energy (enthalpy) on a polycrystalline Ni surface -4.91 eV/atom [47]. In this way, a large energy difference occurs in the FS segregation energies of S between our calculation (-2.91 eV/atom) and the experimental data (-1.41 eV/atom). At this stage, it is not clear whether the estimation of the binding energy in the inner bulk is sufficient or not since we restrict the binding site to only the 6 site and the direction of relaxation to only along the *c* axis. As for the binding energies at the GB/FS, there may be a large dependence on the characteristics of GB/FS structures as stated above and shown in table 1. For those reasons, both the binding energies in the inner bulk and at the GB/FS should be investigated in more detail. However, these are problems in the next stage since the first purpose of this paper is to reveal general trends for many elements.

In table 2, we also show the GB/FS segregation energy for the elements N, O, Si, In, Sn, and Sb. Again, the overall trends are similar for the calculated and experimental data, although the experiments were mainly done on the GBs and FSs of Fe except for the In case.

3.3. Comparison with previous theoretical works

We show the resulting embrittling potency energies in table 3, with those calculated by the other authors [9, 10]. In our calculation, the embrittling potency energies are found to be -0.94 (-0.84) eV/atom for B, -0.22 eV/atom for C, -0.13 (-0.01) eV/atom for P, and 1.06 eV/atom for S for the non-magnetic (magnetic) case. The values for B and C are negative, meaning that they strengthen the GB, while the value for S is positive, meaning that it weakens the GB. These results are in agreement with the general trends found in the experiments [40, 41, 44] and the other calculations [5, 9, 10, 19]. Sn (0.59 eV/atom) and Sb (1.06 eV/atom) atoms are calculated to be embrittlers in Ni, which is similar to the experimental observations that these atoms were embrittlers in Fe [3]. The effects of Sn and Sb on the IGHE of Ni were also observed experimentally [40, 41]; Sn was not deleterious, but rather beneficial, while Sb was deleterious, but the size of its effect was about half that of S. In our calculations, Sn has a little larger embrittling potency energy than H, which seems to be inconsistent with the above experimental results. However, the sizes of the energies are rather close for H and Sn. The experimental trend that Sb is a stronger embrittler than Sn is at least consistent with our calculated results. In addition, the GB segregation energy of Sb is about half that of S in our calculations. This may be related to the experimental fact that the deleterious effect of Sb is about half that of S.

Table 3. The calculated binding energies (E_{b0} and E_b) and embrittling potency energies (ΔE_{b0} and ΔE_b) in units of eV/atom for some elements. Here, E_{b0} and ΔE_{b0} are calculated using GB0 and FS0 sites, while ΔE_b is calculated using the most stable GB and FS sites that are shown below. The left arrow indicates that the most stable site is the 0 site. The positive/negative value of embrittling potency energy means that the solute atom has an embrittling (E)/strengthening (S) effect on the Ni $\Sigma 5$ GB. The comparison with previous works is shown.

	E_{b0}			E_b				
Solute	GB0	FS0	ΔE_{b0}	GB/site	FS/site	ΔE_b	Effect	References
H[a]	−2.99	−3.26	0.27	—	—	—	E	Geng [9]
H[a]	−2.11	−2.47	0.36	−2.38/1i	−2.78/1i	0.40	E	This work [11]
H	−2.18	−2.50	0.32	−2.46/1i	−2.82/1i	0.36	E	This work [11]
He[a]	—	—	2.50	—	—		E	Smith [10]
He	2.94	−0.02	2.96	2.76/1e	←	2.78	E	This work
Li	—	—	1.25	—	—	—	E	Smith [10]
Li	−0.88	−2.08	1.20	−1.22/1e	←	0.86	E	This work
B[a]	−6.83	−6.34	−0.49	—	—	—	S	Geng [9]
B[a]	−7.14	−6.30	−0.84	←	←	←	S	This work
B	−7.41	−6.47	−0.94	←	←	←	S	This work
C	−8.20	−7.87	−0.33	←	−7.98/1i	−0.22	S	This work
N	−7.50	−7.85	0.35	−7.97/1i	−8.63/1i	0.66	E	This work
O	−5.79	−6.66	0.87	−5.91/1i	−7.39/1i	1.48	E	This work
P[a]	−5.66	−6.36	0.70	—	—	—	E	Geng [9]
P[a]	−6.45	−6.44	−0.01	←	←	←	None	This work
P	−6.79	−6.66	−0.13	←	←	←	Weak S	This work
S	−4.72	−5.78	1.06	←	←	←	E	This work
Ca[a]	—	—	7.26	−/1	—	1.20	E	Smith [10]
Ca	1.59	−2.79	4.38	−1.34/1	←	1.45	E	This work
Sn	−1.44	−3.56	2.12	−2.97/1	←	0.59	E	This work
Sb	−2.19	−4.36	2.17	−3.30/1	←	1.06	E	This work

[a] Spin-polarized calculations.

The embrittling potency energy for P is negative or almost zero, which is opposed to the other theoretical result (0.7 eV/atom) obtained by Geng *et al* [9, 10] and the experimental views that P (and S) is one of the most common impurities having a detrimental effect on nickel-based alloys. Nevertheless, there are some experimental arguments that P is an embrittler in Fe but seems to be *not* one in Ni [48]. The first example is that the IGHE of Ni is suppressed in the presence of P atoms in the experiments by Bruemmer *et al* [40] and Ogino *et al* [41]. To be precise, they did not suggest that P is a cohesion enhancer of the Ni GB. Bruemmer *et al* suggested that P segregated strongly to the GBs in Ni and limited the enrichment of harmful sulfur; they estimated that the size of the deleterious effect of S was about fifteen times larger than that of P, while Ogino *et al* suggested that P (and B) suppressed the IGHE of Ni, assisted by oxygen; this was in addition to Bruemmer's suggestion. These features imply at least that the embrittling effect of P on the GBs in Ni is much smaller than that of S and/or O. (According to Ogino *et al*, oxygen has a deleterious effect on the hydrogen embrittlement of nickel GBs. This is consistent with our result: that the embrittling potency energy of oxygen is positive and large (1.48 eV/atom) as shown in figure 8 and table 2.) The second one is the beneficial effect of P on stress rupture life and the improvement in ductility of Ni alloy 718 [49], although in this case the interactions between P and some alloy elements cannot be negligible. Whether P in Ni is an embrittler or not is at least a subtle problem in the Rice–Wang model [3], since it is reported that the FS segregation energy of P (S) would be dependent on the character of the Fe (Ni) surface planes as shown in table 1 and that the GB segregation energy of P would

also be dependent on the Fe GBs [39]. If this is true, this analysis will be complex, since the embrittling potency would be dependent on the types of both the GBs and the FSs.

As Geng *et al* estimated the embrittling potency energy to be about 0.7 eV/atom for P [9] using the same exchange–correlation functional GGA(PBE96) as us, we have checked the accuracy of our calculation in several ways: using a larger cut-off parameter in the basis functions, including spin polarization, employing a larger unit cell (GB: 28 Ni layers; FS: 15 Ni layers), etc. However, our result did not change significantly. In addition, we have performed a preliminary calculation for this Ni–P system using the Vienna *ab initio* simulation program VASP [50–52] with PAW–PBE potentials. Using the same unit cells (20 Ni layers for GB and 11 Ni layers for FS systems), the final result on the embrittling potency energy of P atom is found to be very similar—about −0.11 (−0.06) eV/atom for non-magnetic (magnetic) systems. These results do not change significantly when we allow relaxation in the *ab* plane or use larger unit cells (30 Ni layers for the GB and 15 Ni layers for the FS system). Thus, at this stage, we can at least say that the embrittling potency is much stronger for S than P. In fact, this agrees with the experimental trends [40, 41, 49].

Table 3 summarizes the calculated binding energies and embrittling potency energies for some solute atoms; part of this was also dealt with previously by Geng *et al* [9] and Smith *et al* [10]. Note that these previous works have treated the binding energies and embrittling potency energies with a limited number of GB/FS sites (mostly GB0 and FS0 sites), while the present work deals with those for several more sites (GB0, GB1, GB1i, GB1e, FS0, and FS1i). Whether each solute has an embrittling or strengthening effect has been judged from the sign of the embrittling potency energy. We can see that our judgments on the embrittling/strengthening effects for the solute atoms are in agreement with those in previous works, except in the case of the P atom.

Now, we make a comparison in detail. For H atoms, the final embrittling potency energy is in good agreement (−0.27 versus −0.40 eV/atom). Although we can see large discrepancies in the binding energies (E_{b0}) for both GB0 and FS0, these are due to the difference between the estimations of the total energy of an isolated H atom, $E_{tot}(H)$. In our case, it is estimated using a fcc supercell only for the hydrogen case as stated in the previous section. On the other hand, they (Geng *et al*) probably estimated it from a monolayer calculation for the paramagnetic state (0.5 electronic occupation in both up and down spin states), though they did not mention this in their paper [9]. As a result, our calculated binding energy at the most stable FS1i site is −2.78 eV/atom, which is in excellent agreement with the experimental energy of adsorption on the Ni(111) surface (−2.90 [36], −2.87 eV/H [35]) as shown in our previous paper [11]. For B and P atoms, the binding energies for FS0 cases, especially in the spin-polarized state, are in excellent agreement with the previous work [9]. However, our binding energies at the GB0 site are calculated to be appreciably lower than values from the previous work [9]. (This might be because the geometry optimization of the GB structure has been done more successfully in our calculation than theirs. See below.) As a result, our embrittling potency energies are estimated to be lower for the B atom. For the same reason, the embrittling effect of the P atom, which was seen in the previous result [9], disappeared in our calculation. For He, Li, and Ca atoms, embrittling potency energies are in good agreement except for the ΔE_{b0} case for Ca.

While the atomic relaxation and lattice expansion around the GB plane are almost negligible for the H atom, they become larger as the atomic radius of the solute becomes larger (B < P < Ca). This is seen particularly for the GB0 configuration as in figure 5. Thus, our calculations seem to give larger reductions in the total energies than the previous calculations [9, 10] when the solute atom has a great effect on the geometrical change around the GB plane. One of the possibilities for explaining this discrepancy is related to the geometry optimization procedure using the force minimization method which may be trapped in the

energetic local minimum configuration. Force minimization procedures restricted to only the *c* axis direction may fail to give the correct global minimum configuration for some cases. In addition, the inclusion of spin polarization may have some effects on the optimized geometry. Even when we calculated the binding energies in the spin-polarized state for the H, B, and P cases, we performed the geometry optimization in the spin-polarized state but starting from the optimized structure for the non-spin-polarized state. In fact, there are subtle differences between the previous work [9] and our result in the calculated interlayer distances for the B and P cases. When a P atom is at a GB0 site, for example, their results (our results) in units of au are 2.20 (2.33), 1.40 (1.49), 1.26 (1.39), 1.54 (1.58), and 1.32 (1.43), for GB1–GB2, GB2–GB3, GB3–GB4, GB4–GB5, and GB5–GB6 interlayer distances, respectively. These differences are appreciably larger than those for the clean GB or hydrogen included GB cases as shown in our previous paper [11]. The second possibility is in the method of calculation for the GB systems: the use of a two-dimensional isolated slab model sandwiched by two vacuum regions or a three-dimensional unit cell with a periodic boundary. However, these should be the same if the system size is large enough, and as we have mentioned previously, we have checked that the size effect in the direction of the *c* axis is small, at least in our three-dimensional unit cell. For these reasons, a more detailed and systematic study including spin polarization, using larger unit cells, and using a different code (VASP), are now in progress.

4. Conclusions

In this paper, we performed first-principles calculations (basically in the non-spin-polarized state) of the binding energies of solute atoms in inner bulk Ni, on the Ni(012) surface, and at the Ni $\Sigma 5$ (012) symmetrical tilt grain boundary. The binding energies at both the substitutional and interstitial sites were calculated for a series of solutes of non-transition elements between H and Rn. The electronic structure calculation is done using WIEN2k code, which is based on the FLAPW method within the generalized gradient approximation. For each calculation, interlayer distances are optimized by force minimization. The binding energy difference between the GB/FS site and the inner bulk site defines the GB/FS segregation energy, and the segregation energy difference between the GB and the FS defines the embrittling potency energy according to the Rice–Wang model and the previous calculations [1].

It has been shown that the GB and FS segregation energies are negative for most of the non-transition elements. This means that most of the solutes can segregate to the GB and FS, since they bind more strongly to the GB/FS site than to the inner bulk sites. The embrittling potency energies are positive for most solutes, meaning that the solute segregation to the GB causes embrittlement. However, there are some exceptions for which embrittling potency energies are negative and large, namely, Be, B, C, and Si atoms. These elements are characteristic in that they tend to form covalent bondings with Ni metal. They are predicted to be cohesion enhancers in Ni $\Sigma 5(012)$ GB, in contrast to the other solutes.

Our calculated GB/FS segregation energies were compared with experimental data. Although there are some difficulties for the comparison, at least the order of magnitude was in good agreement. The calculated GB/FS segregation energies for H, B, C, P, S, Sn, and Sb were $-0.31/-0.71$, $-2.37/-1.43$, $-0.83/-0.61$, $-1.76/-1.63$, $-1.85/-2.91$, $-0.91/-1.50$, and $-0.86/-1.92$ eV/atom, and the resulting embrittling potency energies were 0.40, -0.94, -0.22, -0.13, 1.06, 0.59, 1.06 eV/atom, respectively. (Here, these values are for the spin-polarized case for H and for the non-spin-polarized case for the others.) Within a physical picture of simple site competition (neglecting the interactions between the solutes), the interrelations of the size of the calculated GB/FS segregation energies and embrittling potency energies for these solute elements were consistent with various experimental findings: S has a detrimental effect on the intergranular hydrogen embrittlement (IGHE) of Ni while B

has a beneficial effect and reduces the effect of S; B does not influence the FS segregation of S on the Ni surface [42]; P has a beneficial effect on the IGHE of Ni similarly to B [40, 41]; C must have a smaller GB segregation energy than S [43] and decrease the extent of the IGHE of Ni [44]; and the deleterious effect of Sb on the IGHE of Ni is much larger than that of Sn [41]. It seems not to be possible to explain the effect of Sn, which improves the resistance to the IGHE of Ni [41]. However, at least the embrittling potency energy of Sn (0.59 eV/atom) is much closer to that of H (0.40 eV/atom) than to those of the other harmful solutes such as S (1.06 eV/atom) and Sb (1.06 eV/atom).

Our calculated embrittling potency energies were compared with the previous first-principles works [9, 10] in detail. The signs of the embrittling potency energies are in good agreement except for the P atom. While P had an embrittling effect in the previous works, in which its embrittling potency energy was 0.70 eV/atom for the spin-polarized case, this disappeared and the result was a value of −0.13 (−0.01) eV/atom for the non-spin-polarized (spin-polarized) case in our calculations. Our result seems to be more consistent than theirs with the beneficial effect of P on the IGHE of Ni [40] and on the mechanical properties of nickel-based alloy 718 [49]. However, it is a subtle problem for various reasons as stated in the previous section. For example, the interactions between P and the other elements at the GB/FS and/or the dependence of the embrittling potency energies on the characteristics of the GB/FS structures should be investigated before drawing a conclusion.

In this paper, we showed the overall trend for the non-transition elements embedded in Ni. Similar calculations for the transition elements embedded in Ni and more detailed calculations including spin-polarized states are now in progress and will be published elsewhere.

We finally point out that it is also important to study the solute segregation of Fe GBs by means of first-principles calculations. However, there are some difficulties in the calculations to be overcome: inclusion of the spin polarization in the interaction between Fe and the solute is inevitable, and the insertion of light solute atoms at interstitial sites has to be treated more carefully than in the fcc case.

Acknowledgment

We thank Dr Tsukada and Dr Miwa (JAERI) for helpful discussion. The calculations were mainly performed on the Origin 3800/256CPU system and partly on the MPP system in JAERI CCSE.

References

[1] Wu R, Freeman A J and Olson G B 1994 *Science* **265** 376
[2] Wimmer E, Krakauer H, Weinert M and Freeman A J 1981 *Phys. Rev.* B **24** 864 and references therein
Weinert M, Wimmer E and Freeman A J 1982 *Phys. Rev.* B **26** 4571
[3] Rice J R and Wang J 1989 *Mater. Sci. Eng.* A **107** 23
[4] Wu R, Freeman A J and Olson G B 1994 *Phys. Rev.* B **50** 75
[5] Wu R, Freeman A J and Olson G B 1996 *Phys. Rev.* B **53** 7504
[6] Zhong L, Wu R, Freeman A J and Olson G B 2000 *Phys. Rev.* B **62** 13938
[7] Geng W T, Freeman A J and Olson G B 2000 *Phys. Rev.* B **62** 6208
[8] Zhong L, Wu R, Freeman A J and Olson G B 1997 *Phys. Rev.* B **55** 11133
[9] Geng W T, Freeman A J, Wu R, Geller C B and Raynolds J E 1999 *Phys. Rev.* B **60** 7149
[10] Smith R W, Geng W T, Geller C B, Wu R and Freeman A J 2000 *Scr. Mater.* **43** 957
[11] Yamaguchi M, Shiga M and Kaburaki H 2004 *J. Phys. Soc. Japan* **73** 441
[12] Shiga M, Yamaguchi M and Kaburaki H 2003 *Phys. Rev.* B **68** 245402
[13] Geng W T, Freeman A J and Olsen G B 2001 *Phys. Rev.* B **63** 165415
[14] Wang L G and Wang C Y 1998 *Comput. Mater. Sci.* **11** 261
[15] Yang R, Yang Y M, Huang R Z, Ye H Q and Wang C Y 2002 *Phys. Rev.* B **65** 94112
[16] Shang J X and Wang C Y 2002 *Phys. Rev.* B **66** 184105

[17] Hu Q M, Yang R, Xu D S, Hao Y L, Li D and Wu W T 2003 *Phys. Rev.* B **67** 224203
[18] Lu G L and Kioussis N 2001 *Phys. Rev.* B **64** 24101
[19] Janisch R and Elsässer C 2003 *Phys. Rev.* B **67** 224101
[20] Cottrel A H 1990 *Mater. Sci. Technol.* **6** 807
[21] Blaha P, Schwarz K, Sorantin P and Trickey S B 1990 *Comput. Phys. Commun.* **59** 399
[22] Blaha P, Schwarz K, Madsen G K H, Kvasnicka D and Luitz J 2001 *WIEN2k, An Augmented Plane Wave +Local Orbitals Program for Calculating Crystal Properties (Karlheinz Schwarz, Techn. Universität Wien, Austria)* ISBN 3-9501031-1-2
[23] Perdew J P, Burke K and Ernzerhof M 1996 *Phys. Rev. Lett.* **77** 3865
[24] Sanderson R T 1962 *Chemical Periodicity* (New York: Reinhold)
[25] Sutton L E (ed) 1965 Table of interatomic distances and configuration in molecules and ions *Special Publication No. 18* Suppl. 1956–1959 (London: Chemical Society)
[26] Huheey J E, Keiter E A and Keiter R L 1993 *Inorganic Chemistry: Principles of Structure and Reactivity* 4th edn (New York: HarperCollins)
[27] Porterfield W W 1984 *Inorganic Chemistry, a Unified Approach* (Reading, MA: Addison-Wesley)
[28] James A M and Lord M P 1992 *Macmillan's Chemical and Physical Data* (London: Macmillan)
[29] References [24–28, 30, 31] are cited in http://www.webelements.com/
[30] Allred A L 1961 *J. Inorg. Nucl. Chem.* **17** 215
[31] Pauling L 1960 *The Nature of the Chemical Bond* 3rd edn (Ithaca, NY: Cornell University Press)
[32] Eichler A, Mittendorfer F and Hafner J 2000 *Phys. Rev.* B **62** 4744
[33] Stuckless J T, Wartnaby C E, Al-Sarraf N, Dixon-Warren St J B, Kovar M and King D A 1997 *J. Chem. Phys.* **106** 2012
[34] Lassila D H and Birnbaum H K 1986 *Acta Metall.* **34** 1237
[35] Wonchoba S E and Truhlar D G 1996 *Phys. Rev.* B **53** 11222
[36] Christmann K, Behm R J, Ertl G, Van Hove M A and Weinberg W H 1979 *J. Chem. Phys.* **70** 4168
[37] Stafford S W and McLellan R B 1974 *Acta Metall.* **22** 1463
[38] McLean D 1957 *Grain Boundaries in Metals* (Oxford: Oxford University Press)
[39] Lejček P, Hofmann S and Paidar V 2003 *Acta Mater.* **51** 3951
[40] Bruemmer S M, Jones R H, Thomas M T and Baer D R 1983 *Metall. Trans.* A **14** 223
[41] Ogino Y and Yamasaki T 1984 *Metall. Trans.* A **15** 519
[42] Ladna B and Birnbaum H K 1988 *Acta Metall.* **36** 745
[43] Larere A, Guttmann M, Dumoulin P and Roques-Carmes C 1982 *Acta Metall.* **30** 685
[44] Kimura A and Birnbaum H K 1988 *Acta Metall.* **36** 757
[45] Siegel D J and Hamilton J C 2003 *Phys. Rev.* B **68** 94105 and references therein
[46] Yin M T and Cohen M L 1984 *Phys. Rev.* B **29** 6996 and references therein
[47] Miyahara T, Stolt K, Reed D A and Birnbaum H K 1985 *Scr. Metall.* **19** 117
[48] Zhang Y, Zhu F and Xiao J (C Hsiao) 1991 *Scr. Metall.* **25** 1617
[49] Dong J, Zhang M, Xie X and Thompson R G 2002 *Mater. Sci. Eng.* A **328** 8 and references therein
[50] Kresse G and Hafner J 1993 *Phys. Rev.* B **48** 13115
[51] Kresse G and Furthmüller J 1996 *Comput. Meter. Sci.* **6** 15
[52] Kresse G and Furthmüller J 1996 *Phys. Rev.* B **54** 11169
[53] Liu C M, Nagoya T, Abiko K and Kimura H 1992 *Metall. Trans.* A **23** 263
[54] Suzuki S, Obata M, Abiko K and Kimura H 1983 *Scr. Metall.* **17** 1325
[55] Grabke H J 1986 *Steel Res.* **57** 178
[56] Papazian J M and Beshers D N 1971 *Metall. Trans.* **2** 491
[57] Shelton J C, Patil H R and Blakely J M 1974 *Surf. Sci.* **43** 493
[58] Was G S and Martin J R 1985 *Metall. Trans.* A **16** 349
[59] Grabke H J 1987 *Chemistry and Physics of Fracture* ed R M Latanision and R H Jones (Dordrecht: Martinus Nijhoff) p 388
[60] Guttmann M 1983 *Atomistics of Fracture* ed R M Latanision and J R Pickens (New York: Plenum) p 465
[61] Suzuki S, Tanii S, Abiko K and Kimura H 1987 *Metall. Trans.* **18A** 1109
[62] Qudar J 1980 *Mater. Sci. Eng.* **42** 101
[63] Muschik T, Gust W, Hofmann S and Predel B 1989 *Acta Metall.* **37** 2917
[64] Seah M P and Lea C 1975 *Phil. Mag.* **31** 627
[65] Guttmann M 1980 *Phil. Trans. R. Soc.* A **295** 169
[66] Guttmann M 1975 *Surf. Sci.* **53** 168
[67] Dumoulin Ph and Guttmann M 1980 *Mater. Sci. Eng.* **42** 249